Improved Characterization of Hydrogen Fuel Cell Membranes

Matthew Garayt

Supervisor: Dr. Barbara J. Frisken

Department of Physics

Simon Fraser University

(Dated: May 5, 2019)

I characterized the morphology of a hydrogen fuel cell membrane commercially known as Nafion. First generation Nafion (N112/N115) was compared with the second generation (N211) at various temperatures and humidities to examine their structural differences. The membranes were analyzed in a new humidity- and temperature-controlled chamber (Xenocs) using small angle X-ray scattering (SAXS) at temperatures ranging from 30–80°C and relative humidities (RH) between 30–90%. The Kapton chamber windows were characterized to allow for proper background subtraction of Kapton intensity profiles, and folded and not folded membrane samples were compared to determine an easier method for mounting. Equilibration time for changes in the Nafion structure after an RH change of 30 and 40% were observed to be of the order of 30 minutes. The membrane profiles at different RH were fit to a multi-peak pseudo-Voigt function with a constant offset and negative power law at low Q (reciprocal space) values, with a clear ionomer peak (0.2 $Å^{-1}$) appearing above 40% RH for N115 and 30% RH for N112 and N211. The membranes were also analyzed using dynamic vapour sorption (DVS) at 80°C; N211 showed a significantly higher increase in water uptake than N112/N115.

I. INTRODUCTION

In this project I studied the effects of hydration on the micro- and nanoscopic structure of Nafion, the standard for polymer electrolyte membranes (PEMs) in hydrogen fuel cells. The PEM performance and stability is tied to its transport and mechanical properties, and are correlated with interactions between chemical structure and water uptake during morphological change. The equilibrium behaviour and properties are affected by the chemical

and mechanical energies of the system; in other words, the interplay between hydration and structure deformation. Therefore, understanding this balance and how it changes with both types of Nafion and varying environmental conditions (humidity and temperature) is of great importance.

PEMs are one of five major types of fuel cell electrolytes, the others being: solid oxide fuel cells; alkaline fuel cells; phosphoric acid fuel cells; and molten carbonate fuel cells [1]. The PEM-type fuel cell comprises the ion-containing polymer-based (ionomer) proton-conducting electrolyte membrane sandwiched between platinum-containing electrodes, with hydrogen gas pumped into the anode and oxygen gas into the cathode. The hydrogen molecules are oxidized at the anode; electrons flow through an external circuit and return at the cathode while protons conduct through the PEM and meet the electrons and oxygen molecules at the cathode. Each oxygen atom is reduced and gains two protons (hydrogen ions), forming water. The focus of this project was on the PEM itself, which must at the same time have a high resistance to electron flow while allowing proton conduction, as well as work under various temperature, pH, and hydration conditions.

Using Nafion samples from both generations of production, any differences in structure and water uptake can be examined. The first generation Nafion is manufactured using a melt-extrusion process while the second generation was made with a dispersion casting method, resulting in the former being structurally anisotropic compared to the latter [2]. This has previously been shown to cause anisotropic swelling [2], as well as differences in water uptake, particularly relative humidity (RH) greater than 60% [3]. Dynamic vapour sorption (DVS) is used to examine the water uptake of the PEMs as a function of humidity, which can help in identifying differences observed in the small angle X-ray scattering (SAXS) profiles of the two generations [3]. Moreover, the results obtained are compared against published literature to examine the effectiveness of the humidity chamber.

Another purpose of this project was to study a new humidity chamber and compare to previous results for Nafion. This humidity chamber is an add-on to the current Xenocs SAXS instrument in 4D Labs and will provide helpful information on structure changes in Nafion and other PEMs when hydrated.

II. MATERIALS

Nafion was the first commercialized PEM and is classified as a perfluorinated sulfonic acid (PFSA) ionomer. It consists of a tetrafluoroethylene (Teflon) backbone and perfluorovinyl ether side chains terminating in sulfonate ionic groups [3] as shown in Fig. 1. The M^+ ion is typically an H^+ ion, though this may be substituted for another alkali metal.

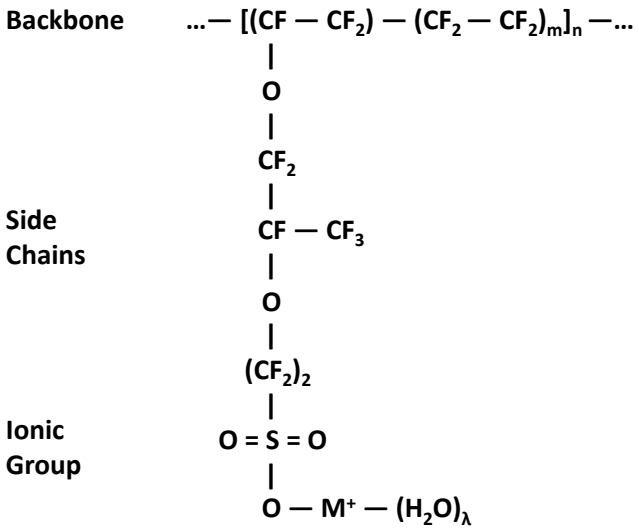

FIG. 1: Chemical structure of Nafion. Adapted from Kusoglu and Weber [3].

The equivalent weight (EW) of Nafion is calculated using either of two equations: first, $\mathrm{EW} = 100m + \mathrm{MW}_{\text{side chain}}$ [3], where m is the number of TFE units in the backbone, as shown in Fig. 1, and $\mathrm{MW}_{\text{side chain}}$ is the side chain molecular weight; second, $\mathrm{EW} = m_{\text{pol}}/n_{\mathrm{SO_3}}$ where m_{pol} is the mass of the polymer in grams and $n_{\mathrm{SO_3}}$ is the number of moles of sulfonate.

Nafion is named using a three digit sequence with the last digit representing the thickness in thousandths of an inch (mil) [3]. For example, Nafion 117 (N117) indicates a material that is 7 mil thick. The first generation of Nafion begins with "11" to signify the EW of 1100 $\mathrm{g_{pol}/mol_{SO_3}}$ [2, 3], but the second generation, "21", does not follow this trend and can have an EW between 990 and 1100 $\mathrm{g_{pol}/mol_{SO_3}}$ [2, 4].

As discussed previously, a melt-extrusion process is used to manufacture the first generation Nafion. Melt-extrusion is the processing of polymeric materials above their glass transition temperature (200°C for Nafion [2]) to effect molecular level mixing of polymers and active compounds. This creates an orientation of the polymer chains compared to the dispersion casting procedure of the second generation [2], which disperses Nafion in its

acidic form in alcoholic solvents and tape-casts it into membranes. Thus the melt-extruded, first generation Nafion has anisotropic swelling while the dispersion-cast second generation's swelling is isotropic [2]. As well, second generation Nafion has slightly higher water uptake above 60% RH and proton conductivity over the first generation [2–4], perhaps as a result of the relative isotropy [2].

The swelling of the Nafion membrane is a complex, multistep process caused by the interactions between the water, hydrophilic ionic moieties, and the hydrophobic polymer matrix [3]. Governed by the solvation energy of the ionic groups and chemical potential of the water molecules to connect with the hydrophilic ionic moieties, the water uptake process is balanced by the deformation of the ionomer's hydrophobic matrix [3], hence the chemical-mechanical energy balance.

To adequately compare samples of various age and source, a preconditioning technique was used [5]: each film was submerged in 1 M HCl for 2 hours; 1 M NaOH for another 2 hours; and then boiled in distilled and deionized water for another hour. This has several consequences: first, it cleans any dirt from the surface of the films; second, it makes the M^+ in the ionic group an Na^+ ion [6]; and third, the boiling erases the thermal history of the film [3]. The preconditioning also causes changes in the water uptake, transport coefficients, density, permeability, ionic conductivity, selectivity, mechanical properties, thermal stability, phase-separated nanostructure and/or crystallinity, surface topology, and energy [3]. Thus to compare results between other studies and my own, the same preconditioning method should be used. After preconditioning, the films were dried under vacuum at room temperature ($\sim$21 $^{\circ}$C) overnight.

III. METHODS

A. Nafion Water Uptake and DVS

Upon exposing the membrane to water, it will uptake water until saturated. The water uptake, λ, is related to the macroscopic uptake through the EW of the membrane [3],

$$\lambda = \frac{n_{H_2O}}{n_{SO_3}} = \frac{\Delta m_{H_2O}\,\mathrm{EW}}{m_{pol}\,MM_{H_2O}}, \tag{1}$$

where n_i is the number of moles of species i, m_i is the mass of species i, and MM_{H_2O} is the molar mass of water. Water uptake can be explored both in water adsorption and

desorption. In water adsorption, the Brunauer-Emmett-Teller (BET) theory equation used by Takata *et al.* [7] based on a finite layer analysis assumes Langmuir adsorption where water vapour adsorbs as a monomolecular layer on the membrane, with water clusters then forming on the already present monomolecular layer. Water desorption, on the other hand, is likely limited by the rate of interfacial transport across the membrane-gas interface [8]. This means there is an expected hysteresis between adsorption and desorption isotherms because the mechanism for adsorption and desorption are different [9].

The water uptake of a membrane is affected not only by its intrinsic chemical and physical structure, but also the temperature of the preconditioning, as well as age and contamination [3]. These factors affect the chemical-mechanical energy balance of the ionomer's phase separated nanostructure, either affecting the backbone rigidity or propensity to dissolve. Moreover, samples are exposed on the order of an hour to a given humidity, reaching an apparent equilibrium. However, the relaxation times for many polymer characteristics are much longer (possibly years) than most experiments and thus the membrane is considered to be in a quasi-equilibrium [3].

Exploring the water uptake of Nafion is done using DVS. DVS measures the mass change of a sample as a function of time and RH at a constant temperature, elucidating how much and how quickly it adsorbs and desorbs water. One can then use Eq. 1 to convert the mass absorbed to water uptake λ, yielding the adsorption and desorption isotherms. Experimentally, a balance is enclosed in a humidity and temperature controlled chamber with one side of the balance holding the sample to be tested and the other a reference sample. A polynomial is fit to data with $0\% < \mathrm{RH} < 20\%$, but generally one is more interested in $20\% < \mathrm{RH} < 100\%$ where the following function fits best,

$$\lambda = a + b\,\mathrm{RH} + c\exp\left(d\,\mathrm{RH}\right), \tag{2}$$

where the fit parameters are determined by least-squares fitting [4]. This is a phenomenological model, no physical meaning is assigned to the fit parameters [4].

Sample composition can also be described by the polymer volume fraction ϕ_{pol} instead of λ [5]. However, one can convert between the two forms using

$$\phi_{\mathrm{pol}} = \frac{\overline{V}_{\mathrm{pol}}}{\lambda\overline{V}_{\mathrm{H_2O}} + \overline{V}_{\mathrm{pol}}}, \tag{3}$$

where $\overline{V}_{\mathrm{pol}}$ and $\overline{V}_{\mathrm{H_2O}}$ are the molar volume of the polymer and water, respectively. The

molar volume is defined as

$$\overline{V}_{\text{pol}} = \frac{MM_{\text{pol}}}{\rho_{\text{pol}}}, \tag{4}$$

where MM_{pol} is the molar mass and ρ_{pol} is the density of the polymer; $\rho_{\text{pol}} = 2.1$ g/cm^3 [5], and the density of water at 25°C is 0.997 g/cm^3. However, the molar mass of the polymer is not known as the total size of the backbone, the n in Fig. 1, is proprietary.

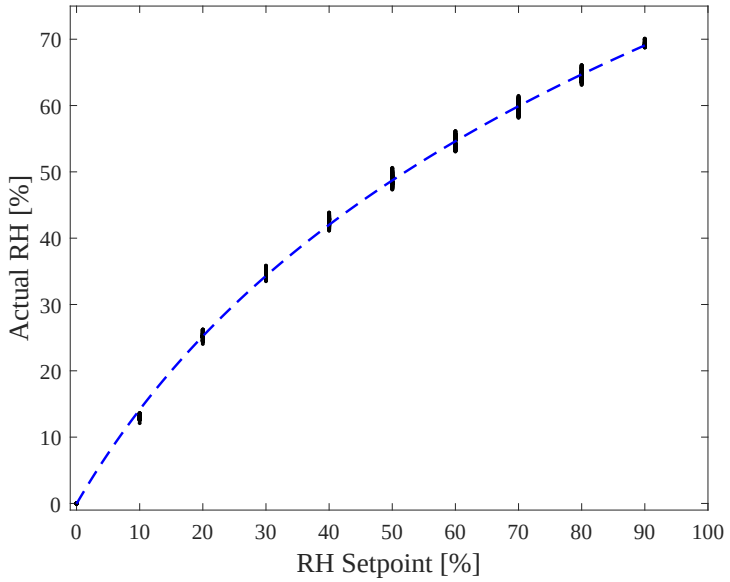

FIG. 2: DVS humidity chamber RH measured value versus setpoint, with a logarithm with constant offset fit as the dotted line.

The DVS data was obtained by Kingsly Wu in Dr. Steven Holdcroft's group in SFU Chemistry. The DVS humidity chamber used to collect data on the water vapour sorption of our Nafion samples has a significant variation in the setpoint relative humidity to the measured RH at 80°C over a 46 hour period. Figure 2 shows the RH was set at 10% intervals between 0 and 90%, and it would ideally be linear so that the actual RH is the setpoint; however, it is clearly nonlinear. The fit to the data is a of a logarithm with constant offset $y = a \log(x + b) + c$ with $a = 50.7 \pm 0.3$, $b = 31.0 \pm 0.3$, and $c = -174 \pm 2$ with the error being the 95% confidence bound. The χ^2_{red} is 0.01 using the standard deviation of the actual RH at each setpoint, indicating the error on the data was overestimated. The results in Fig. 2 are important because it shows the physical limits on the equipment that, if one simply looked at the setpoint, may miss in a more cursory check of the data. By comparison, the temperature values varied mostly within 1°C of the 80°C setpoint.

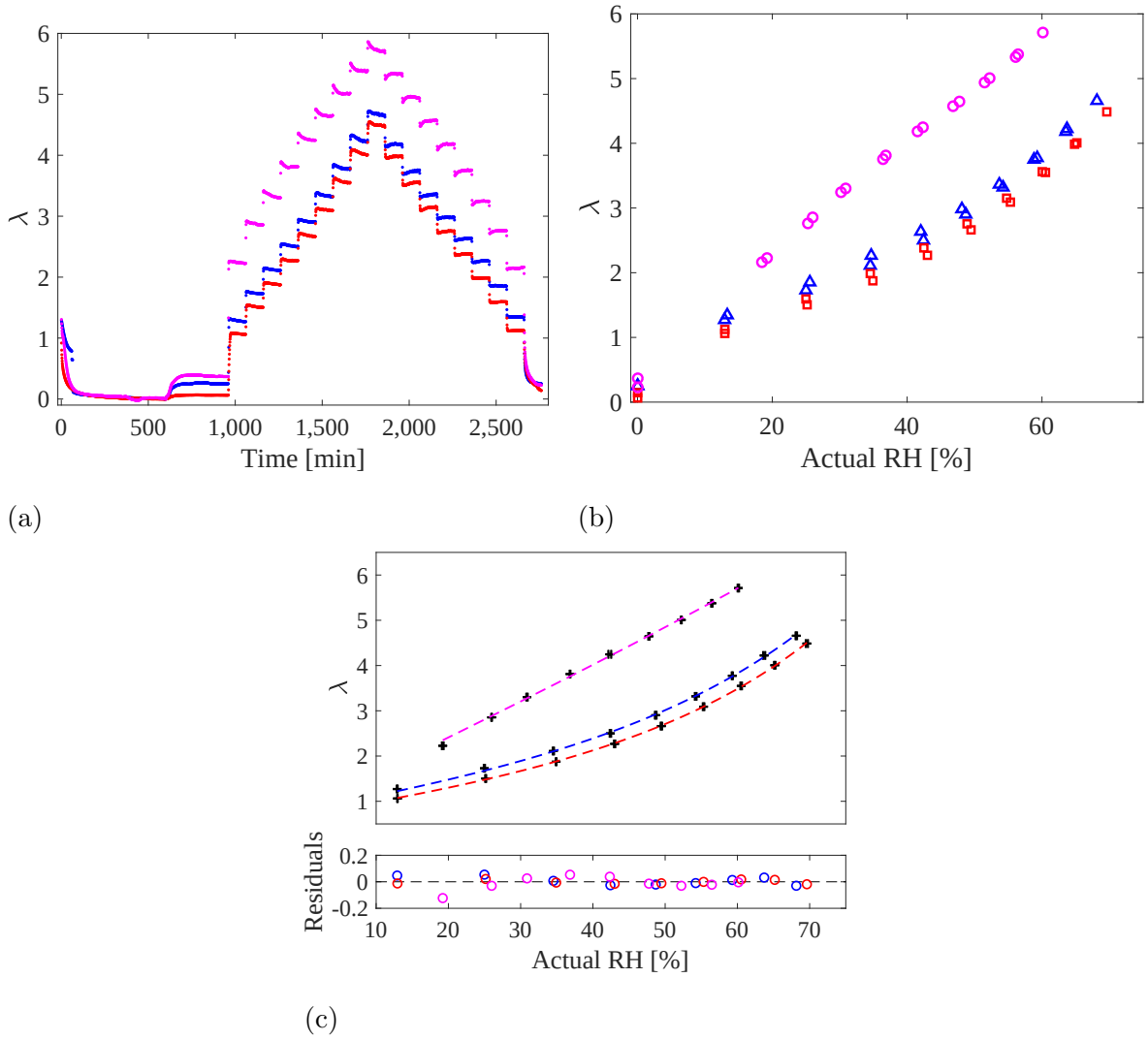

FIG. 3: (a) shows the film water uptake λ as a function of time for N112 (blue), N115 (red), and N211 (magenta) at 80°C, (b) shows λ as a function of RH without error bars with both the adsorption and desorption isotherms, and (c) shows only the adsorption data (black) with a fit to Eq. 2 (dotted lines) at 80°C with residuals.

The water uptake as a function of time is shown in Fig. 3a as the RH changes in steps. Each step in RH lasted 99 min with a measurement every minute, other than the initial 0% RH which lasted for 959 min, and it is clear that after the initial change in RH the value of λ settles to an equilibrium value. Thus the final 10 min were averaged to get the results shown in Fig. 3b. This gives the most accurate possible measurement of λ for the time that was allowed for the measurements because it can take months for Nafion to equilibrate [3]. The data given is for the mass of the polymer as it uptakes water, so using Eq. 1 with

EW = 1100 g_{pol}/mol_{S0_3} and MM_{H2O} = 18 g/mol.

The water uptake λ of the N112 (blue triangles), N115 (red squares), and N211 (magenta circles) films as a function of RH is plotted in Fig. 3b and shows both the adsorption and desorption isotherms. For both N112 and N115 in Fig. 3b, the water uptake increases nonlinearly with relative humidity, so the amount of water adsorbed between 20 and 30% RH is much lower than between 60 and 70% RH. This is expected from water uptake analyses in previous studies [2–4, 7, 10]. Also, there is an observable hysteresis on desorption (upper curve) compared to adsorption (lower curve) that is maximal at a difference of 0.15 for N112 and 0.11 for N115 around 34.5% RH. At lower and higher RHs than 34.5%, less of a hysteresis is present. The hysteresis between adsorption and desorption is expected because the mechanisms for adsorption differ from those in desorption as previously mentioned [7–9]. As well, the first generation Nafion has anisotropic swelling due to its melt-extruded manufacturing which causes hysteresis in water uptake [2]. Moreover, the N112 and N115 isotherms show similar curvature and mostly differ by a constant offset in water uptake. This is perhaps due to the two films adsorbing different amounts of water under ambient conditions.

The DVS measurements for N211 in Fig. 3b show that unlike the first generation Nafion, λ is nearly linear with relative humidity, indicating that second generation Nafion can uptake similar amounts of water at each humidity. Also, the N211 sample appears to have little hysteresis from adsorption to desorption, with only a clear difference of 0.14 in water uptake at 0% RH. This is striking as it indicates that around operating temperature (80°C), within a wide range of RHs from 20 to 60%, the adsorption and desorption of water for N211 is symmetric. This could indicate that the adsorption and desorption rates are much closer than for the first generation Nafion, which could be because thinner films have a higher desorption rate [8]. Peron *et al.* also performed a DVS study of N211 and found less hysteresis between the adsorption and desorption isotherms than the first generation Nafion [2]. They speculated that this is due to the dispersion casting fabrication method that creates relatively isotropic swelling compared to the first generation Nafion [2]. Finally, the water uptake at RH 0% is again nonzero, which is perhaps because the sample was not completely dry to begin the measurements.

It is also evident that all films in Fig. 3b have nonzero water uptake even at zero RH, with N211 having more uptake at zero. N112 has $\lambda = 0.25$ at zero RH for both the adsorption and

desorption isotherms, while N115 has $\lambda = 0.06$ on adsorption and $\lambda = 0.15$ on desorption, and N211 has $\lambda = 0.23$ on adsorption and $\lambda = 0.37$ on desorption. This may again indicate that the samples adsorbed water prior to the experiment, but also shows some water remains trapped after desorption. The increased λ at 0% RH for N211 may be due to the increased water uptake overall, so in the same ambient humidity it adsorbs the most water.

Nafion	a	b [1/%]	c	d [1/%]
N112	0.6 ± 0.2	0.02 ± 0.05	0.2 ± 0.8	0.04 ± 0.04
N115	0.6 ± 0.2	0.02 ± 0.02	0.1 ± 0.3	0.04 ± 0.02
N211	0 ± 10	0.1 ± 0.3	0 ± 10	0.0 ± 0.8
N115 [4]	0.759	0.04944	0.00016	0.117430

TABLE I: DVS adsorption best fit parameters to Eq. 2 from Fig. 3c (first three rows) and the Maldonado *et al.* paper [4]. The uncertainties in the first three rows represent the 95% confidence bounds.

The adsorption isotherms for the three PEMs were fitted to Eq. 2 to produce the plots in Fig. 3c. My error bars in Fig. 3c were based on the standard deviation of the water uptake during the last 10 min at each RH, but is likely an underestimate of the true error. The fit function fits N115 the closest, though in the three cases the residuals are relatively small (most on the order of 10^{-2}) as compared to the variation in the total dataset and are evenly distributed about zero. Both the N112 and N115 fits have parameters within error of one another, showing that the water uptake for both samples is nearly identical, as expected since they are both first generation Nafion and differ only in thickness and perhaps age. For both fits, the 95% confidence bounds are on the same order as the parameters themselves, indicating the fits have significant error because the error in water uptake at each point is on the order of 10^{-4}, thus resulting in the fits being less significant than they may appear to the eye. Maldonado *et al.* [4] did not report on errors of their best fits or any goodness-of-fit statistics; however, the error bars on their λ data were on the order of 1 (one hundred times larger than mine), so while their fit did appear to deviate more from the data points, it was still within the error bars.

Maldonado *et al.* [4] also performed a water uptake analysis of N115 at, among other

temperatures, 80°C. Their reported best fit values without uncertainties are listed in Table I, although they obtained data between 20 and 95% RH, a higher maximum value than mine. Maldonado's a, b, and c fit parameters are within or just outside of the uncertainty of my fits for first generation Nafion, but Maldonado's value for d is larger than either of mine, resulting in their fit appearing almost entirely linear from 20 to 60% RH. Above RH 60%, their fit is nonlinear but has a steeper increase than both of my N112 and N115 samples. The difference in results is likely due to multiple factors: first, the preconditioning method employed by Maldonaldo is different than mine, which has been shown to affect water uptake [3]; second, they did not use DVS but instead placed samples above a saturated salt solution for the desired RH in an oven [4]; third, they allowed for 7 days of equilibration time [4] rather than 99 min as I did; and fourth, their samples were probably a different age, and hence at a different level of crystallization, at the time of measurement than mine.

The fit parameters in Table I confirm the qualitative appearance of the isotherms in Fig. 3: a, c, and d are all zero while b is large in comparison to all other fits. b is the linear slope term in Eq. 2, thus showing that this fit is essentially completely linear with a larger slope than the first generation Nafion. Peron *et al.* [2] also found using DVS that N211 has a mostly linear trend in the water uptake below 80% RH as in Fig. 3c at 25°C.

Overall, the DVS measurements showed that both N112 and N115 uptake similar amounts of water at each RH; however, N211 uptakes more water at each RH. Moreover, the second generation Nafion's water uptake is essentially linear while the first generation's has a high degree of nonlinearity. Finally, my results for N115 show that preconditioning, among other factors such as sample age, affect their water uptake, so I have controlled those variables as best as possible.

B. Xenocs SAXS Instrument

1. About SAXS

To analyze the Nafion films, I employed the Xenocs small-angle X-ray scattering (SAXS) instrument in 4D Labs. The measurements yield intensity peaks corresponding to different length scales of ordering within the PEM (the inverse of Q, the scattering vector defined later) as shown in Fig. 4. The origin of each peak is constructive interference of X-rays

scattering due to different length-scales within the PEM. Below 0.02 $Å^{-1}$, there is the extreme-small-angle X-ray scattering (ESAXS) upturn corresponding to large scale electron density inhomogeneities [5], and the matrix knee around 0.06 $Å^{-1}$, attributed to the distance between the crystalline domains of the polymer matrix [10]. Moreover, one observes the ionomer peak (peak 0) around 0.2 $Å^{-1}$ attributed to the distances of the spherical ionic domains [5, 10], and peak 1 around 1.2 $Å^{-1}$, associated with the backbone-backbone correlation length. Peak 2 around 2.7 $Å^{-1}$ represents overall crystallinity in the membrane [3].

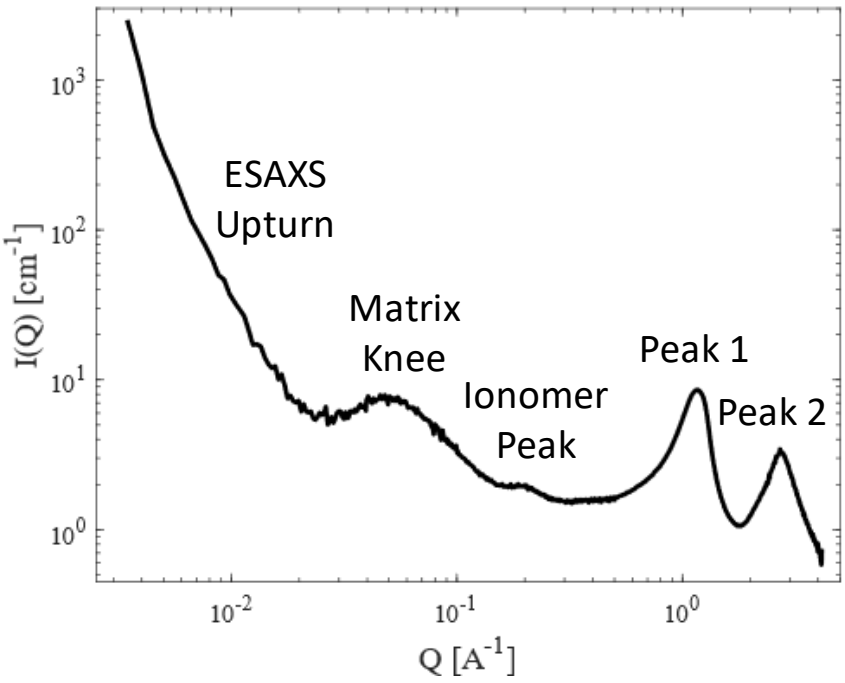

FIG. 4: A log-log plot of the SAXS profile from dry N115 film.

Samples were analyzed both under vacuum in a dry and humidified environment and equilibrated for half an hour when dry and an hour when humidified. Measurement time was usually 10 min for wide-angle X-ray scattering (WAXS) and 30 min for medium-angle X-ray scattering (MAXS). As the Q range decreases (i.e. WAXS to ESAXS), the time for data collection increases because the detector is physically further and at a larger angle, thus fewer photons reach the detector per given time.

The peaks in Fig. 4 appear rather broad, an indication of short-range order; a characteristic of amorphous membranes. Although not having a crystalline lattice, the PEMs can still be studied using X-ray scattering because of this short-range order. Short-range order

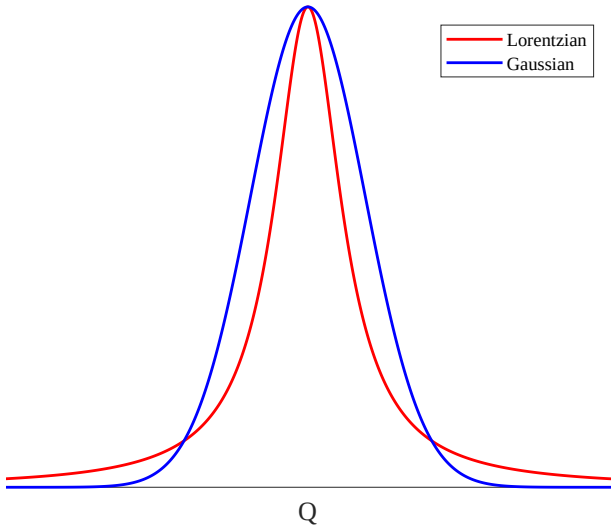

FIG. 5: Lorentzian and Gaussian functions normalized to the same maximum value.

describes the local distribution of atoms, or in this case molecules, due to their interactions such as Van der Waals forces or hydrogen bonding [11]. As well, for large asymmetric molecules like Nafion, the short-range order will have directional effects, but when a radial average is taken it is usually symmetric [11]. The local density often has oscillations that can be modelled by exponential decaying amplitudes [11].

According to the Fraunhofer far-field limit of the Huygens-Fresnel integral, the resulting diffraction pattern of light through an aperture (obstacle) is simply its Fourier transform [12]. The real space characteristics of the sample that act as the aperture for the X-rays are measured in Fourier space, also called reciprocal or k space, but for SAXS the measured quantity is the scattering vector $\mathbf{Q}$, the difference in incident and outgoing k, $\mathbf{Q} = \mathbf{k}_i - \mathbf{k}_f$. This allows for a relatively simple method of either calculating the expected scattering pattern observed based on a model sample, or turning the reciprocal space data into real space results. The former approach is used to explain why short-range order peaks appear broad; as discussed, the local density of molecules can often have exponential decays, and when Fourier transformed become Lorentzian peaks. Long-range order, by contrast, is described by Gaussian functions rather than decaying exponentials, and the Fourier transform of a Gaussian is still Gaussian. A Lorenztian by comparison to a Gaussian in reciprocal space is more broad as shown in Fig. 5, thus why it is indicative of short-range order [11].

Similar to X-ray diffraction used for long-range ordered lattice crystals, X-ray scattering results in (usually) symmetric rings that occur at specific scattering angles 2θ. Braggs' law,

$n\lambda_{\text{X-ray}} = 2d\sin\theta$ where d is the spacing between planes or periodicity in the sample, n is the diffraction order, and $\lambda_{\text{X-ray}}$ is the wavelength of the X-rays, describes which angles correspond to constructive interference and thus stronger scattering peaks. The reciprocal vector $Q = 2\pi/d$, so substituting in Braggs' law for primary scattering ($n = 1$) gives,

$$Q = \frac{4\pi\sin\theta}{\lambda_{\text{X-ray}}}. \tag{5}$$

One can also determine the scattering angle and thus Q given the distance from the centre of the rings X (i.e. the axis of the collimated X-rays) to the sample-detector distance L,

$$\tan 2\theta = \frac{X}{L}. \tag{6}$$

2. *Instrumentation*

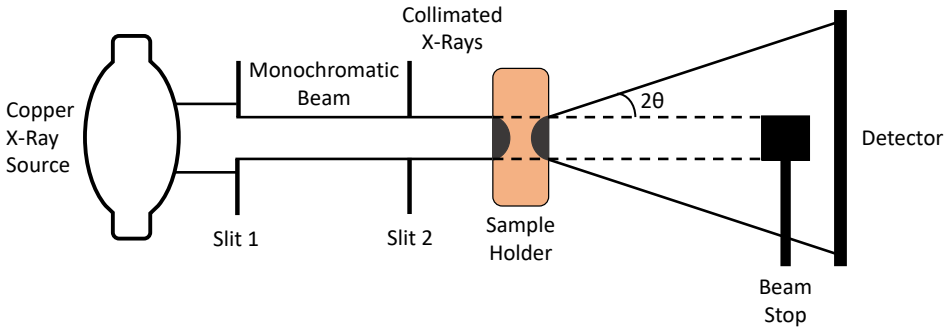

FIG. 6: A schematic of the SAXS instrument. X-rays from the monochromatic copper source are collimated by two slits before scattering off the sample and are collected by the detector.

The Xenocs SAXS instrument uses a copper source to produce the monochromatic X-rays and two slits to collimate the beam as shown in Fig. 6. The X-rays themselves are the copper K_α wavelength (other wavelengths are filtered out before the slits) so are considered monochromatic to simplify scattering calculations. The humidity chamber sample holder has a $\sim$3 mm diameter hole for each sample to allow transmission of the scattered beam. The concentrated beam that is transmitted without appreciable scattering is blocked by the beam stop to protect the detector. The beam stop does introduce two issues: first, it blocks some of the X-rays scattered at very low angles; and second, it must be precisely set to the correct location. The latter is often a problem encountered during setup and must be

Q Range	Minimum Q [Å^{-1}]	Maximum Q [Å^{-1}]
OWAXS	1.96	4.13
WAXS	0.09	2.60
MAXS	0.013	0.70
SAXS	0.005	0.30
ESAXS	0.003	0.20

TABLE II: Q ranges for each configuration of the SAXS instrument.

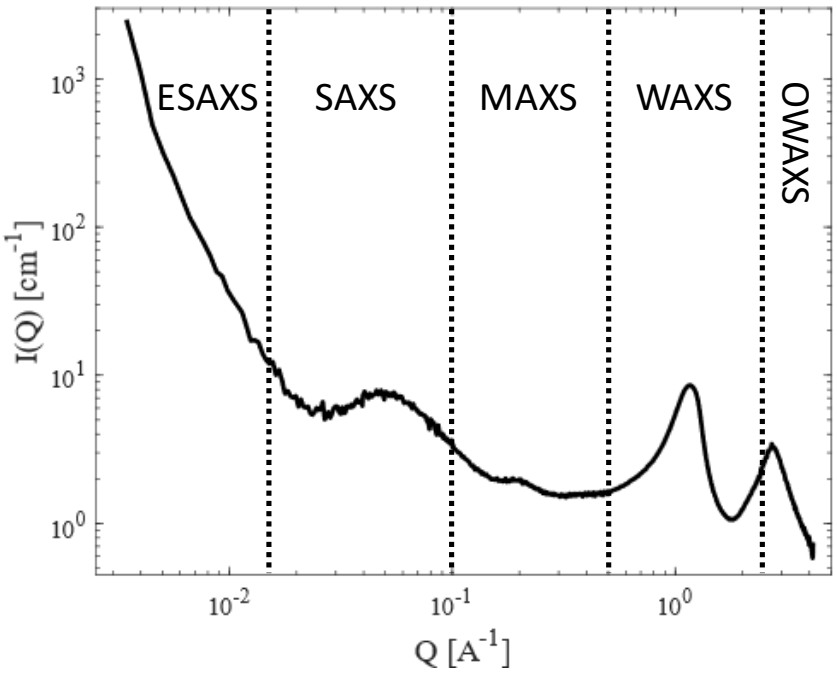

FIG. 7: A log-log plot of the SAXS profile from dry N115 film showing all Q ranges.

carefully adjusted to ensure the beam stop only blocks un-scattered and not the low angle scattered X-rays.

Table II and Figure 7 show the Q ranges available with the SAXS instrument. Each Q range corresponds to a different sample-detector distance, with WAXS having the smallest distance and ESAXS the most. OWAXS is kept at close sample-detector distance, but is offset vertically to capture the extreme-angle scattered X-rays. Each region has a higher degree of noise near the maximum Q values with a greater density of data points towards the maximum when plotted on a logarithmic scale. As well, the data collection time becomes

larger as Q decreases because the detector is further away from the sample and intercepts fewer photons in a given window of time. However, the OWAXS configuration, while constituting the highest Q range, also takes more time than the WAXS configuration because the detector is at a large angle away from the centre of the beam.

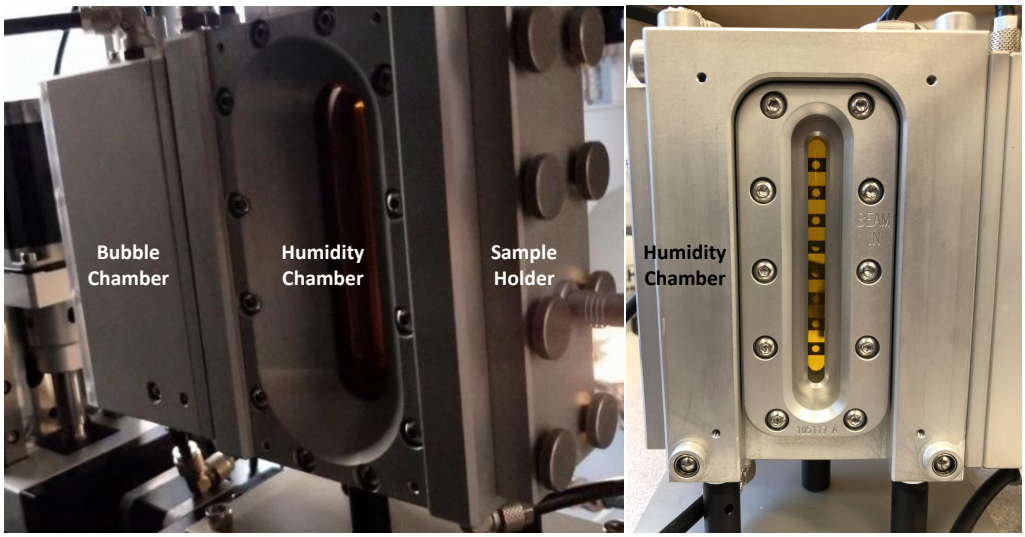

FIG. 8: On the left, the humidity chamber looking toward the X-ray source is composed of the bubble chamber, the humidity chamber itself, and the sample stage. On the right, looking toward the detector, the sample stage inside the humidity chamber is shown within the yellow Kapton windows.

To study PEMs at various RHs and temperatures, I use a humidity chamber supplied by Xenocs shown in Fig. 8. The chamber is comprised of a bubble chamber that contains the proper water-air mixture for the desired RH, a humidity chamber that contains the sample holder in the appropriate RH with Kapton windows to allow X-ray transmission, and access to the sample holder itself. Temperature control is achieved through a water recirculator (heater and chiller) circulating water to heat-exchange with the humidity chamber. All of the water and air connections are made using tubing rated for up to 85°C use and connected by Swagelock connectors. The humidity chamber is connected to a controller box that pumps in dry air and distilled water from a reservoir to the bubble chamber, and is also connected by a serial connection to the humidity chamber's humidity sensor and thermometer. The controller box connects to the PC to allow for user setting and monitoring of the RH and temperature. The humidity chamber is placed in the much larger Xenocs SAXS chamber that is under vacuum to avoid diffraction off of gas (or other airborne) particles.

The humidity chamber sample holder, shown on the right of Fig. 8, can hold at most eight samples, though at least one holder must remain unused for a measurement of the blank transmission. Samples are fixed to the holder by sandwiching between 'dog bone' shaped plates.

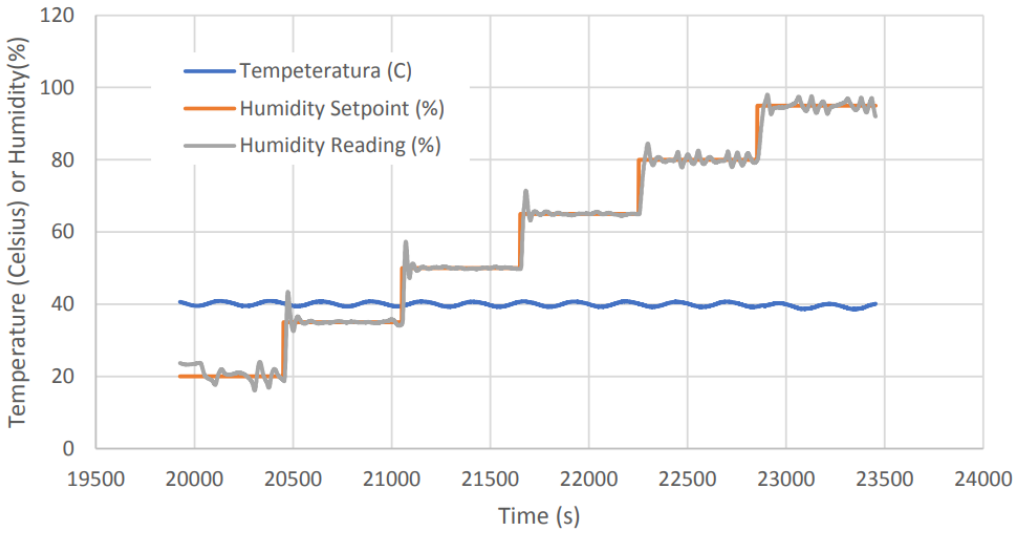

FIG. 9: Humidity and temperature inside the humidity chamber plotted as a function of time with a temperature setpoint of 40°C (from Xenocs manual [13]).

The humidity chamber can be used at an RH of 1% to over 95% at temperatures between 10°C and 70°C [13]. Figure 9 shows the sinusoidal variation of the humidity chamber temperature around the setpoint of 40°C with time, along with the relative humidity's more irregular variation around setpoints between 20 and 95% RH. The stability of the RH is best in the range 30∼70% as shown in Fig. 9, though it varies with temperature and at best the stability is within 1% of the setpoint [13].

I tested the efficacy of the humidity chamber by measuring N112, N115, and N211 and comparing to previously published results. Rubatat *et al.* studied various polymer volume fractions from 95 to 15% of N115 and N117 [5], and Kusoglu *et al.* studied both N117 and 212 between 11 and 100% relative humidity [3, 14]. I measured at RHs between 30 and 90% RH with either a 30 or 40% step, allowing one hour between steps in RH for sample equilibration.

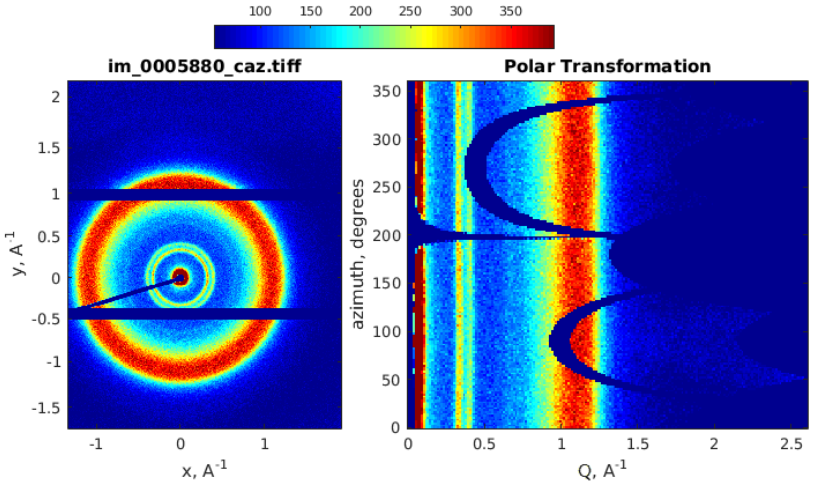

FIG. 10: Raw intensity WAXS data from detector (left) and azimuthal angle intensity profile as a function of Q (right).

3. Measurement

The photon counts (intensity) of the X-rays after passing through the sample are collected on the detector which displays an image as shown on the left of Fig. 10. The image appears as a ring because of the many different orientations of the polymer in the sample, resulting in photons scattering in all azimuthal directions. The detector image is then plotted as a function of azimuthal angle versus Q, but because the beam is not centred on the detector, not all regions have the same amount of data present. The program then averages the intensity over all azimuthal angles and calculates data uncertainties for further analysis.

After averaging the intensity over all azimuthal angles and removal of background scattering (discussed further in the next section), data from different Q ranges can be compared. The raw WAXS and MAXS data for an N112 sample is shown in Fig. 11; there is typically an overlap in the Q ranges. These data should overlap, but there are sometimes discrepancies so the intensities of the two datasets must be scaled to match. The X-rays' intensities in each Q range may differ because of a multitude of factors: the sample may be asymmetric in thickness so at a different detector angle the transmission of photons is different; or various equipment changes like the X-ray source being set to a different potential or the vacuum level or humidity changing. I used my own MATLAB script to stitch together the various Q ranges, aligning all Q range intensities to the WAXS intensity. This is done by matching the intensity of the two Q ranges in the overlapping region by averaging 30 data points from

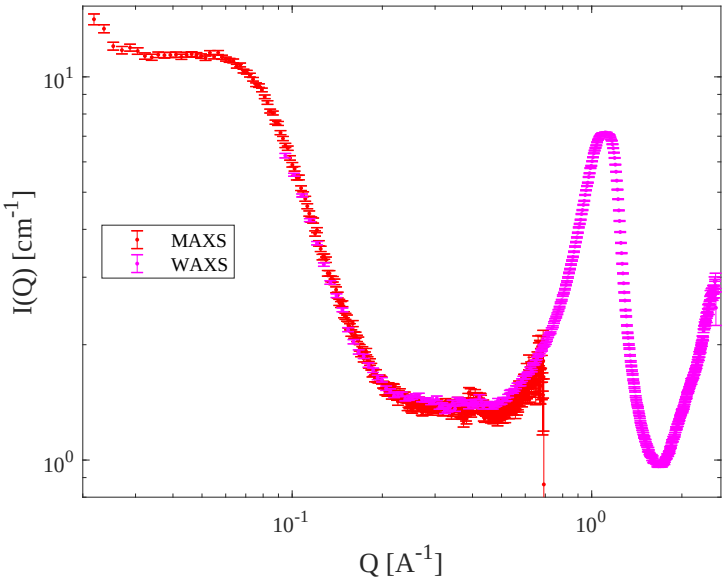

FIG. 11: Raw WAXS (magenta) and MAXS (red) data with error bars representing data uncertainty for an N112 sample.

each range to calculate a scale factor, although at 90% RH this is reduced to 10 data points because the intensity varies more at the overlap of WAXS and MAXS.

4. Instrument Characterization

Before the data can be analyzed, the background scattering is subtracted. In the case of the humidity chamber, background scattering can be due to water condensation, Kapton, or aluminum window peaks among other things. The background subtraction of SAXS data from the final raw data form is $x_f = \frac{x_i}{T_x} - \frac{y}{T_y}$ where x_i is the raw data with the background, T_x is its effective transmission factor measured by the detector (ranges between 0 and 1), y is the raw background data, and T_y is its effective transmission factor (approximately 1). Due to uncertainty in the photon counts on the detector, T_y can be above 1 which is unphysical, but this simply represents a source of measurement uncertainty.

The humidity chamber has two 25 µm Kapton windows. Kapton is strong enough to maintain the sample environment but mostly transparent to X-rays. However, there is scattering due to the windows that must be subtracted as part of the background subtraction. There are eight sample holder positions (1 is at the top, 8 at the bottom), each separated by 10 mm, and initial measurements indicated that the background intensity profile differed by

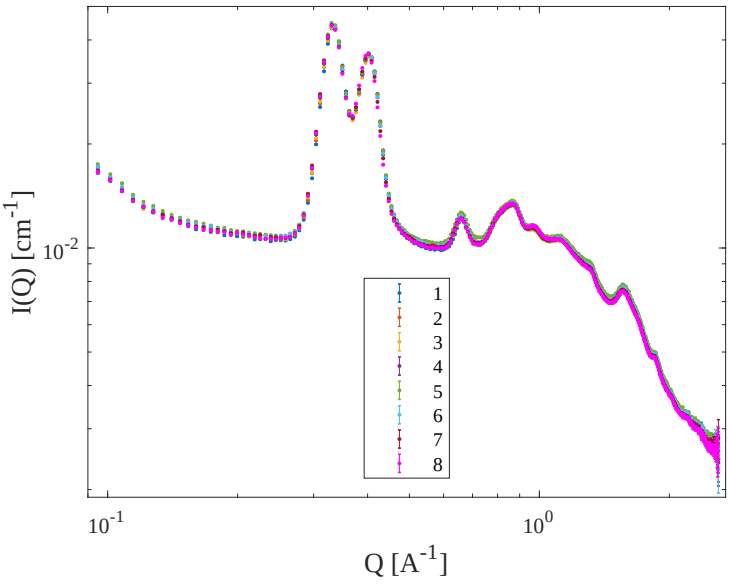

FIG. 12: WAXS profiles of all eight sample holder positions at 30°C without any sample at RH 30%.

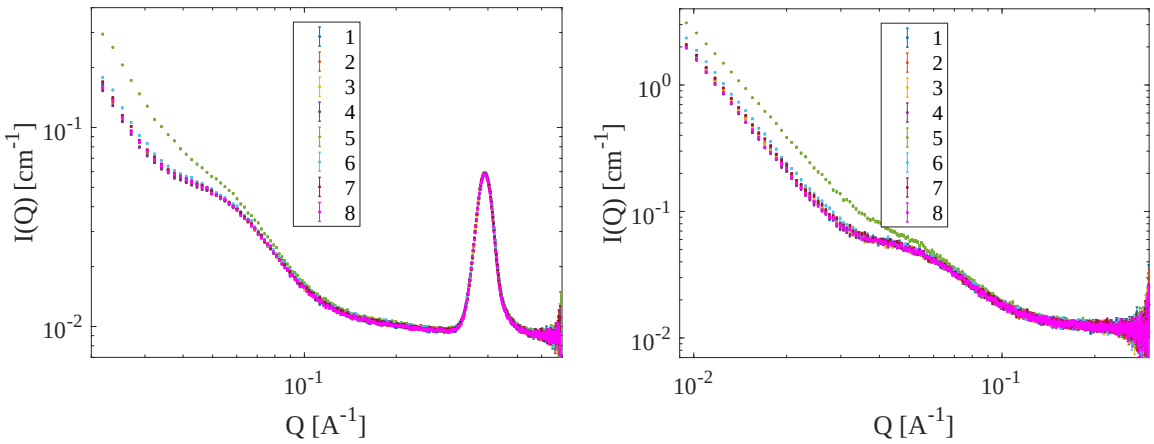

(a) (b)

FIG. 13: (a) MAXS profiles of all eight sample holder positions at 30°C without any sample at RH 30% and (b) shows the same in SAXS.

position. Thus I measured each position at RH 30% and 30°C in the WAXS configuration as shown in Fig. 12. The data reveal a double peak around 0.4 Å^{-1}, which occurs because of the path length difference of X-rays being diffracted by the first and second Kapton windows. While most of the sample holder positions are within error of each other for the entire Q range, sample holder 5 shows a slightly larger intensity than any other.

The higher intensity at sample holder position 5 also presents below 0.06 $Å^{-1}$ as shown in Fig. 13. The peak that appears as a doublet in WAXS around 0.4 $Å^{-1}$ looks like a singlet in MAXS, because the detector position is further away from the sample in MAXS, thus the path length difference becomes a smaller portion of the total path length and it loses resolution. The difference in intensity between position 5 and 7 is more than 1.8 times around 0.022 $Å^{-1}$ (lowest Q in MAXS, mid-to-lower Q in SAXS), its point of maximum variation.

If position 5 is left blank and used for background subtraction of samples in other positions, it erroneously eliminates the low Q upturn normally observed. This may indicate a slight imperfection in the Kapton windows or a thickness difference at position 5, likely occurring from the manufacturing process rather than a change due to increased pressure causing bowing in the windows because that would give rise to a change at more than just one sample holder position. Thus I do not use sample holder position 5 for any measurements.

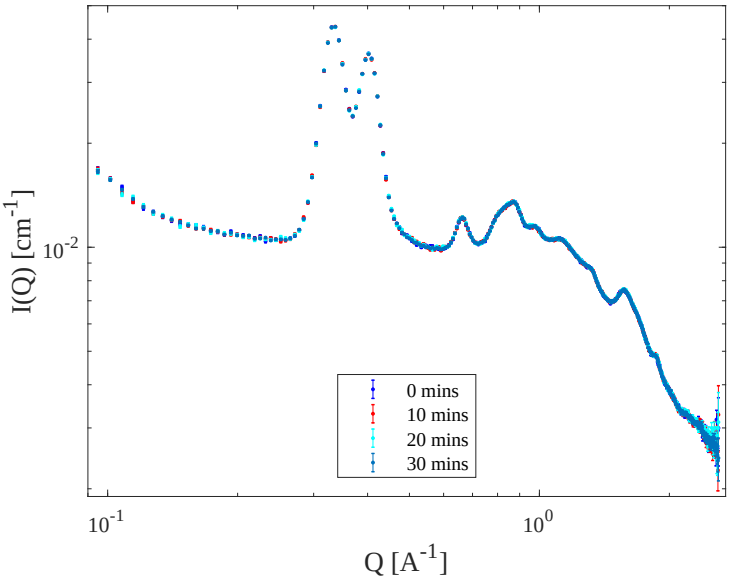

FIG. 14: WAXS profile of the top sample holder position 1 at 30°C without any sample fluctuating around RH 30%.

Another consideration with the Kapton windows is to see if the intensity profile changes as the relative humidity fluctuates. With the humidity fluctuating by 0.7% around the setpoint of 30.0%, there is no noticeable change in the intensity profile over a 30 min period as shown in Fig. 14.

5. *Data Analysis*

To compare the SAXS profiles of Nafion under different conditions, the profiles are fit to a phenomenological model. The morphology, and hence exact form factors, of PEMs including Nafion, is not well known, thus a pseudo-Voigt function is used to describe each peak observed in the SAXS data. A pseudo-Voigt is a linear combination of a Gaussian and Lorentzian peak, thus can describe both short- and long-range order. Along with the peaks, the fitting function includes a constant vertical offset to account for background scattering, and a negative power law for the low Q scattering. The intensity fitting function is then

$$I(Q) = r + a_l Q^p + \sum_{i=1}^{N} \left[s_i a_i \mathrm{e}^{-(2(Q-b_i/c_i)^2)^2 \cdot \log(2)} + \frac{a_i(1-s_i)}{1+2(Q-b_i/c_i)^2} \right], \tag{7}$$

where r is the background term, a_l is the amplitude of the power law with exponent p (typically negative), N is the number of pseudo-Voigt peaks in the fit, s_i represents the shape (i.e. $s_i = 1$ is completely Gaussian, $s_i = 0$ is entirely Lorentzian), a_i is the peak height, b_i is the peak centre position, and c_i is the peak full-width at half-max [15].

To implement the fit, I used MATLAB functions developed by E. M. Schibli [15] that first estimate a value of the background term and power law, then use Gaussians to estimate starting values for the pseudo-Voigt fit. Once the starting values are determined, the pseudo-Voigt fit of Eq. 7 is performed using a Monte Carlo method of nonlinear least-squares fitting over 150 iterations to converge on the best fit values.

A result of a typical fit is shown in Fig. 15, in this case of MAXS and WAXS data for N115 at 40% RH. Equation 7 was used for the fit and the parameters can be found in Table III. The fit has a $\chi^2_{\mathrm{red}} = 1.6$ and the majority of the normalized residuals are within three standard deviations, indicating good agreement with the data.

In the WAXS or large Q region, there is a major peak around 1 Å^{-1} (peak 1) attributed to the backbone-backbone correlation length [15]. This peak was well modelled by three pseudo-Voigt distributions (black, red, magenta), all centred around 1.00 ± 0.19 Å^{-1} and of varying height and full-width at half-max with the rightmost pseudo-Voigt being entirely Gaussian. This peak being entirely Gaussian results from crystallinity in the membrane [3]. Three distributions fit peak 1 best because it is relatively asymmetric and broad.

The next peak around 0.35 Å^{-1} (Kapton peak) in Fig. 15 is an artifact of the Kapton windows of the humidity chamber and is not present in SAXS measurements taken with

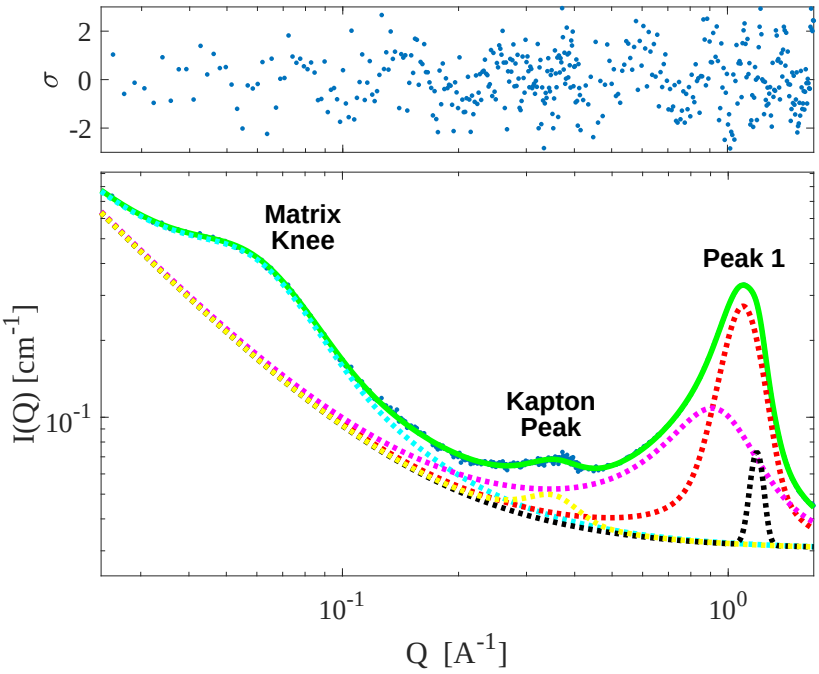

FIG. 15: WAXS and MAXS data of an N115 at 40% RH and 30°C with five peak fit according to Eq. 7 and normalized residuals. Blue points are data, the green solid line is the overall fit, and the coloured dotted lines are each individual peak with the background and power law.

the ambient sample holder. Even with the background subtraction performed in the Xenocs software, there is still a small peak remaining, thus it was fit to a pseudo-Voigt distribution (yellow) as well. The peak itself appears to change shape between the datasets, perhaps the background subtraction may not be as effective in each case, thus subtracting less and having a different shaped peak.

The final broad peak in Fig. 15 around 0.05 $Å^{-1}$ corresponds to the matrix knee and is symmetric along the power law amplitude, thus only one pseudo-Voigt distribution (cyan) is needed to fit it. The matrix knee corresponds to the distance between the crystalline domains of the polymer matrix [10].

All of the individual fits are combined in the total fit in green over the data points in blue shown in Fig. 15. Notice that the ionomer peak is not present in this plot at RH 40%, but is present at higher RHs; in those cases a sixth peak is added.

C. Nafion Characterization

1. *Humidity Equilibration*

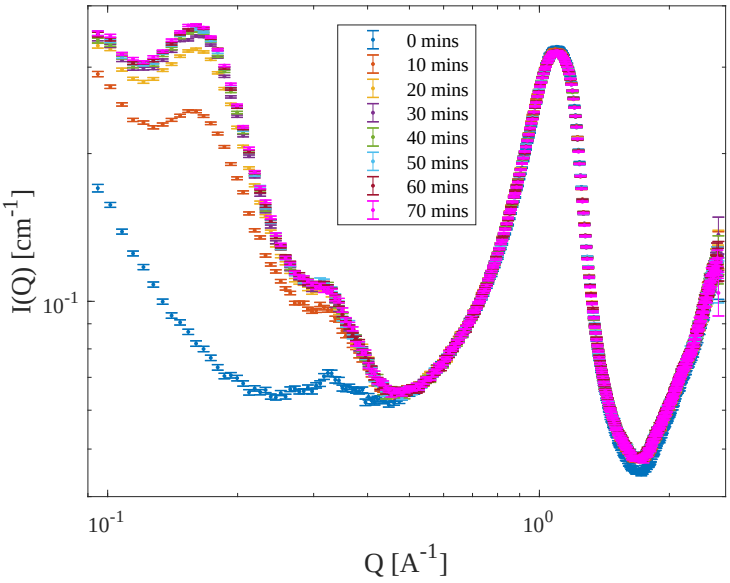

FIG. 16: WAXS data of an N115 sample over 70 min while RH transitions from 40 to 80% at 30°C.

Before exploring how the Nafion structure changes with RH, I studied how much time should be employed between measurements to ensure equilibration. I recorded WAXS profiles of N115 at 10 min intervals for 70 min while changing the RH from 40 to 80%, summarized in Fig. 16. The same procedure was repeated for N211 between 30 and 60% RH and 60 and 90% RH with similar results. The major takeaway from Fig. 16 is that the change in structure of the Nafion in the ionomer peak equilibrates over just 30 min. There is no noticeable change in the scattering pattern observed after this time; however, as previously mentioned, this may simply be a quasi-equilibrium state and a true equilibrium could take orders of magnitude more time to achieve [3].

The major change occurs in the ionomer peak centred around 0.16 Å^{-1}, corresponding to a length of $\sim$39 Å in real space, with negligible changes everywhere else. This increase in the ionomer peak intensity is suggested by Rubatat *et al.* to be a dilution of the scattering entities without a strong structural reorganization of ionic groups [5], although the explanation is debated [3].

An increase in intensity of the ionomer peak of N117 and N211 with increased RH was observed by Rubatat *et al.* [5] and Mochizuki *et al.* [10], respectively, but they also observed a change in the peak to lower Q and the peak was always present even at a ϕ_{pol} of 95% for Rubatat and RH 20% for Mochizuki. Rubatat's data was obtained using a first generation Nafion film with the same preconditioning that I used; however, their sample dates to before 2004 when fluorination of end groups was done to enhance chemical stability [2]. Moreover, because both their Nafion samples were likely years newer at the time of data collection, age may play a role in the data differences.

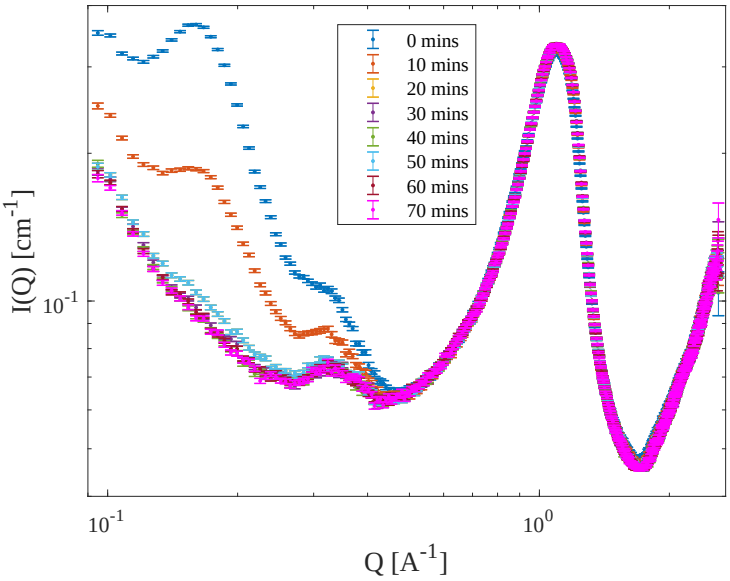

FIG. 17: WAXS data of an N115 sample over 70 min while RH transitions from 80 to 40% at 30°C.

Figure 17 shows WAXS data as the RH was decreased from 80 back to 40%. Again, this was performed with similar results for N211 decreasing from 90 to 30% RH. Interestingly, the ionomer peak intensity becomes depressed and seemingly equilibrates after only 20 min, 10 min faster than for increasing RH. However, the 50 min measurement shows a slight increase in the intensity of the ionomer peak, larger than the error bars but much smaller than the significant changes between 0 and 20 min. This is likely an artifact, perhaps caused by a slight increase in the RH from the two previous measurements which is plausible considering the oscillatory nature of the RH level inside the chamber around the setpoint and the frequent issues with the humidity chamber that were encountered throughout this project. However, due to limitations of the software and measuring overnight, there is not

a record of the humidity values during this part of the data collection, so this hypothesis cannot be tested.

2. *Sample Mounting*

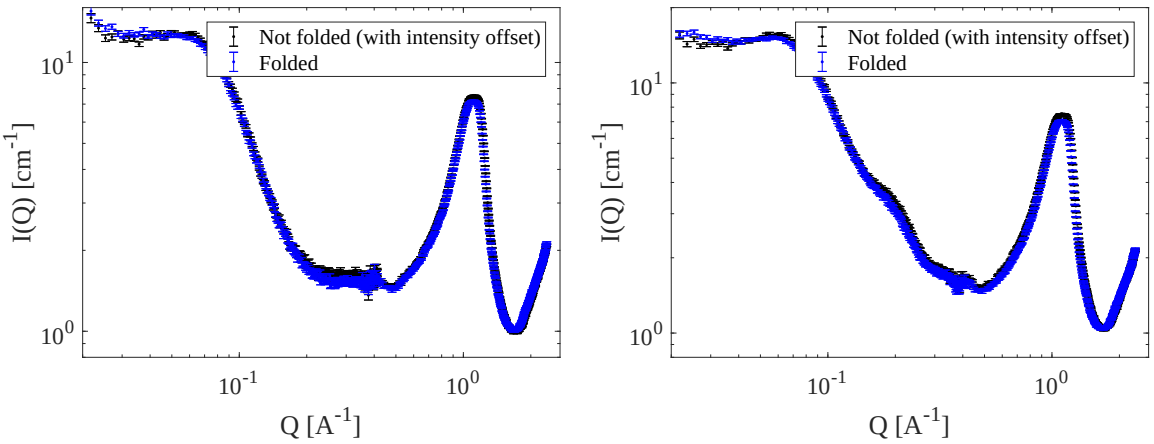

(a) N115 First RH30%

(b) N115 RH60%

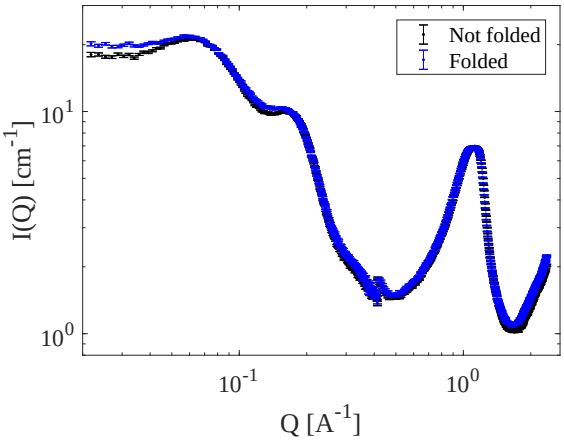

(c) N115 RH90%

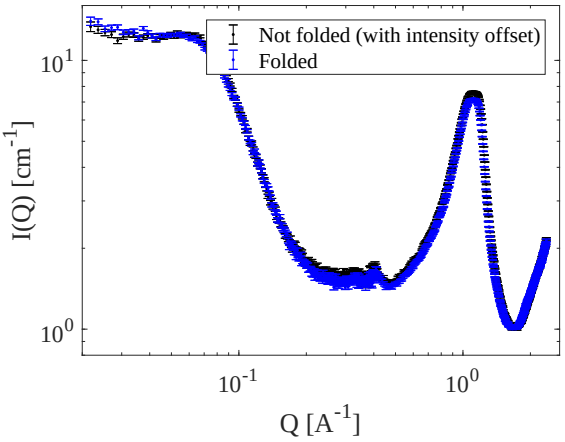

(d) N115 Second RH30%

FIG. 18: (a) WAXS data of two layer N112 folded and not folded at 30°C at RH 30%, (b) 60% RH, (c) 90% RH, and (d) 30% RH again. Intensity offset is to overlay the plots for better comparison due to ∼1% difference in transmission factors.

Because the N112 and N211 samples' thicknesses are only 52 µm and 27 µm, respectively, and the Kapton windows of the humidity chamber are about 25 µm, to obtain a better signal-to-noise ratio I aimed to layer the samples to achieve two layers thick for N112 and two, four, and six layers for N211. Figure 18 compares the intensity profiles for two ways of

mounting samples: one, folding the sample in half; and two, cutting two strips of the sample and stacking them (not folded). These methods were tested because it is easier to mount the folded sample than a stack of cut strips due to electrostatic repulsion. However, there were concerns that stretching, which may occur with folding, may result in changes to the structure. In Figs. 18a, 18b, and 18d, there is no significant difference in either the folded or not folded samples other than the transmission factor, for measurements at both RH 30 and 60%. This indicates that at least below 60% RH, there is no significant structural change due to folding of the sample.

As for the N112 samples at RH 90% in Fig. 18c, there is a slight difference between the folded and not folded samples below about 0.06 $Å^{-1}$. It is not clear why at this elevated humidity there appears to be a small difference in structure that was not present at lower RHs, and assuming it is not an artifact in the data, it could be the result of stretching in the sample due to the folding.

I also compared folded and not folded N211 with two (54 µm), four (108 µm), and six (162 µm). Like the N112 samples that showed little difference between folding and not folding the films, all of the two, four, and six layers of N211 showed little difference, with the two layers plotted in Fig. 19. Only the two layer N211 at RH90% showed a clear difference as shown in Fig. 19c. Below 0.2 $Å^{-1}$, which includes the ionomer peak and matrix knee, the folded sample's intensity is between 7 and 14% larger than the not folded sample. This is likely because the small differences between folded and not folded are exaggerated with more water present, whereas at lower RHs, there is less water so the difference is less evident. This result again supports that using folded samples at and below at least RH60% does not introduce significant error in either first or second generation Nafion. For all other measurements performed in this project, cut and stacked (not folded) samples were used without any folding to avoid any unwanted effects.

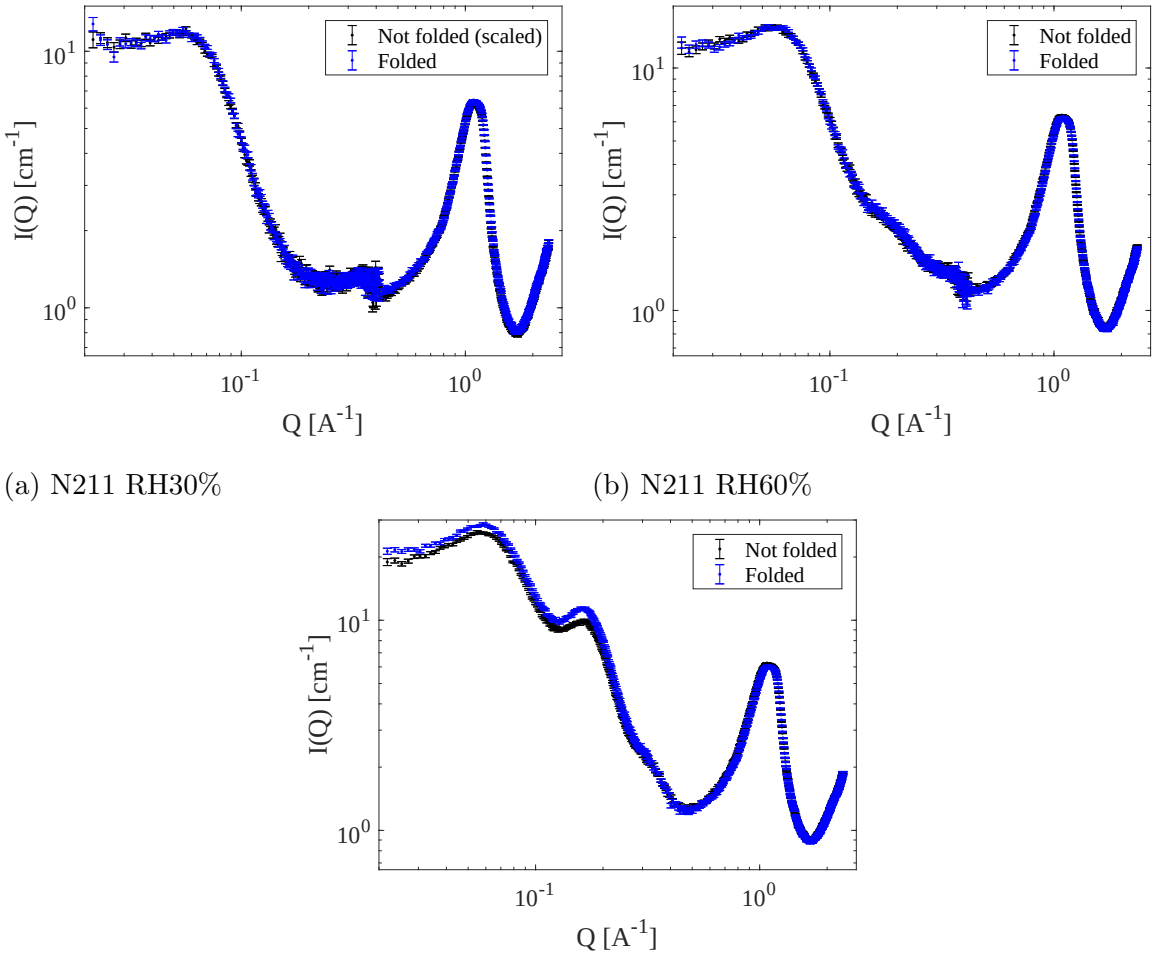

(a) N211 RH30%

(b) N211 RH60%

(c) N211 RH90%

FIG. 19: (a) WAXS data of two layer N211 folded and not folded at 30°C at RH 30%, (b) 60% RH, (c) and 90% RH. Intensity offset is to overlay the plots for better comparison due to incorrect thickness recorded.

IV. RESULTS AND DISCUSSION

All three MAXS and WAXS datasets for N115 at RH 40 and 80% are plotted with fits to Eq. 7 in Fig. 20. The top dataset (blue) is at RH 40% and is the same as the fit in Fig. 15, while the middle (red) is at RH 80% and the bottom is again at RH 40%. This is from the same data collection run as Figs. 16 and 17 where the relative humidity started at 40%, ramped up to 80%, and back down to 40%. Like the fit to the RH 40% data in Fig. 15, the fit to the second RH 40% data uses a five peak pseudo-Voigt and has a $\chi^2_{\text{red}} = 1.6$. However, since there is an additional peak, the ionomer peak or peak 0, for 80% relative humidity, its

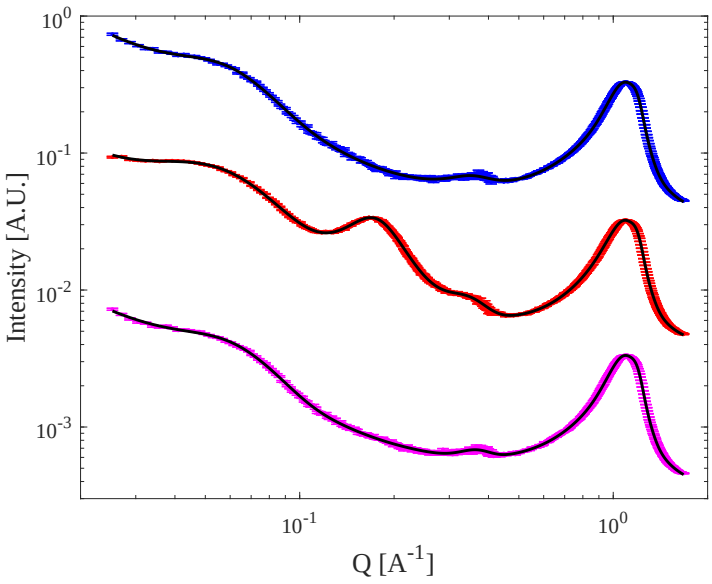

FIG. 20: WAXS and MAXS data and error bars of N115 at RH 40% (blue), 80% (red), and 40% (magenta) at 30°C. A five peak fit to RH 40% (Eq. 7) and a six peak fit to RH 80% are shown as black solid lines.

data was fit using a six peak pseudo-Voigt and has a χ^2_{red} of 1.2. All of the fit parameters for Fig. 20 can be found in Table III.

It appears that in the Q range observed, there is no hysteresis in the structure of the N115 going from RH 40% to 80% and back to 40% as in Fig. 20. This indicates good reversibility in the MAXS and WAXS region of the membrane's structure when subjected to water uptake, so samples can be reused, saving material and reducing cost. It should be noted that the samples are delicate and should be investigated between data collection runs to verify they are still suitable.

Results of N112 and N211 with fits to the data using Eq. 7 are shown in Fig. 21. The fit parameters are recorded in Tables IV and V for N112 and N211, respectively. These fits have slightly larger χ^2_{red} values than those for N115, likely because the subtraction of the Kapton in most of the fits did not leave a clear peak; rather, left more messy data. However, the fits do still represent the data well, with three peaks for the WAXS peak (peak 1) around 1 Å^{-1} and one peak for the ionomer peak (if present) around 0.2 Å^{-1} and the matrix knee near 0.07 Å^{-1}. Just like N115, the three peaks making up peak 1 for both N112 and N211 are centred around 1.00 ± 0.19 Å^{-1} and of varying height and full-width at half-max, again with the rightmost peak being entirely Gaussian. The background constant values are typically

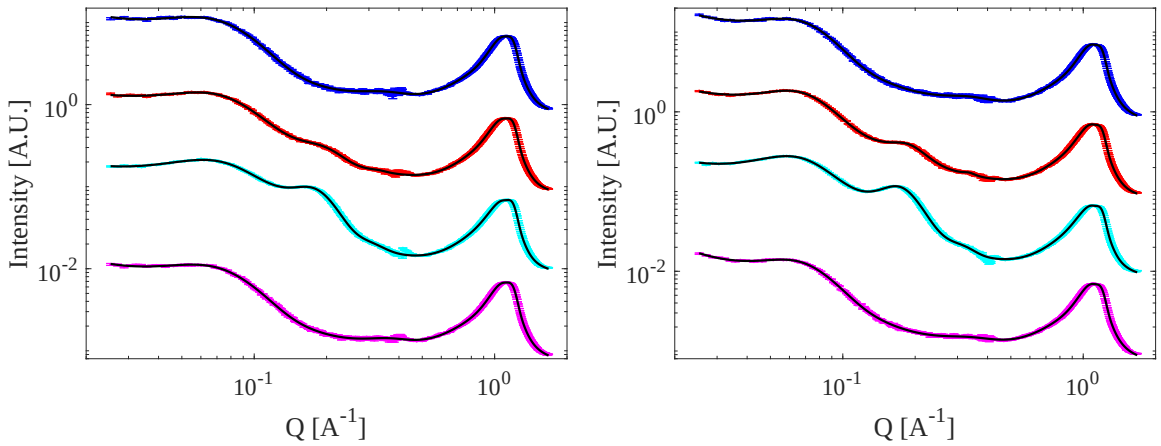

FIG. 21: (a) WAXS and MAXS data of N112 at 30°C at RH 30, 60, 90, and 30% RH again. (b) shows the same for N211. A five peak fit to RH 30% (Eq. 7) and a six peak fit to RH 60 and 90% are shown as black solid lines.

an order of magnitude larger than those for N115, although that is simply a result of using a different thickness of sample, resulting in a different total intensity of X-rays passing through the sample to the detector. Moreover, the height of the peaks and the power law amplitude are an order of magnitude larger as well for the same reason. The power law exponents are all negative, which is as expected for any Nafion membrane at low Q.

The N211 samples also revealed that there is a slight change in the centre position of the ionomer peak upon increasing RH, from 0.18 $Å^{-1}$ to 0.15 $Å^{-1}$ or from 35 to 42 Å in real space. This indicates an increase in spacing between ionic groups, and the peak positions are consistent with the results for N211 in the work by Mochizuki *et al.* even though their results were taken at 80 rather than 30°C [10]. The change in ionomer peak position did not occur with first generation Nafion, so it may show a difference in the structural change between first and second generation Nafion, or may be a result of the improved water uptake for the same RH of the second generation Nafion, which can be linked to its isotropic swelling [2]. Thus the difference between the N115 and N211 may be a result of the N211 simply adsorbing more water than the N115, or the anisotropy in the N115 stifling a change in ionic cluster spacing.

Plotting the d-spacing of the ionomer peak, using $d = 2\pi/Q$, against RH in Fig. 22a, with the matrix knee d-spacing in Fig. 22c, and with the ionomer peak full-width at half

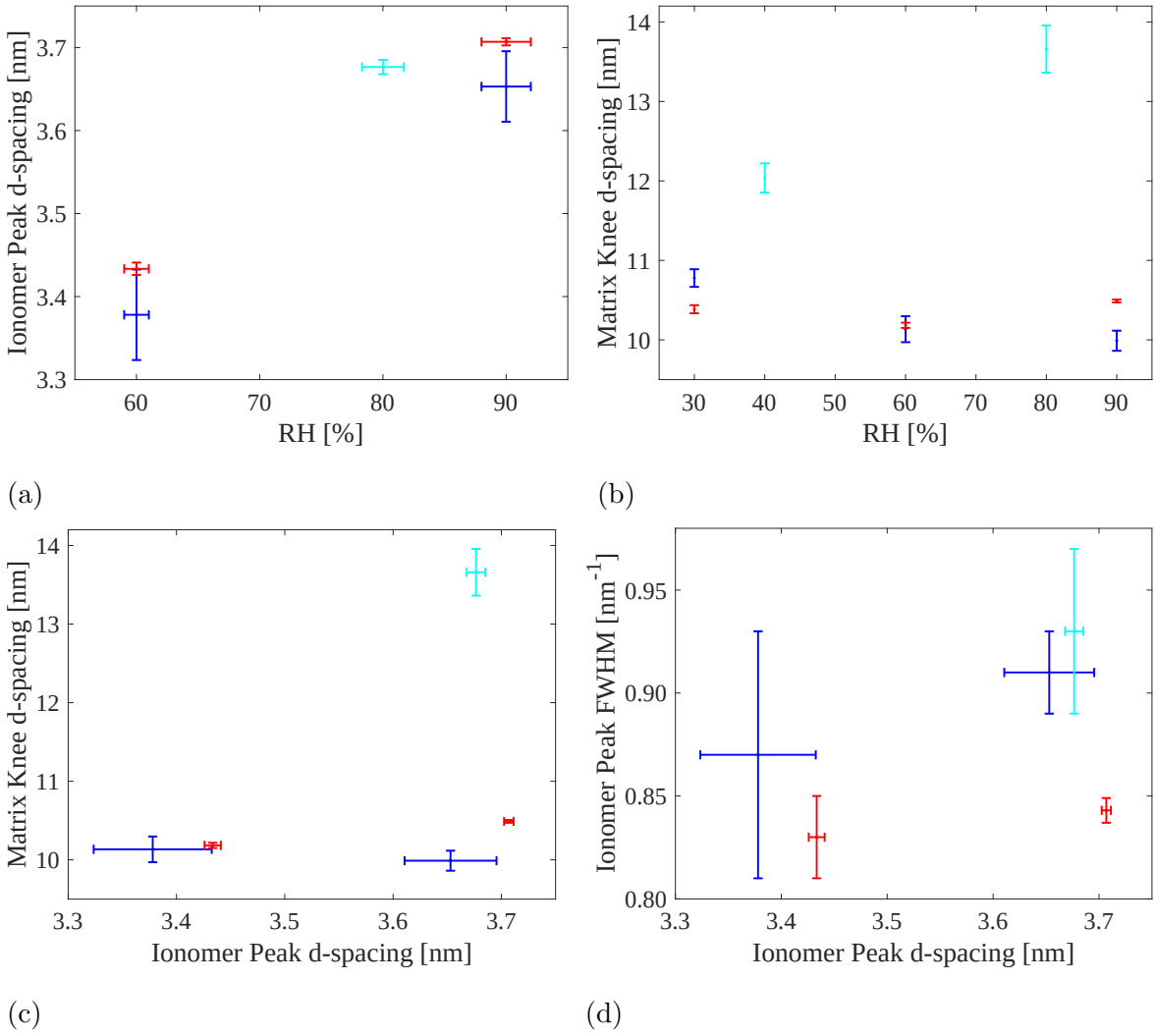

FIG. 22: (a) shows the ionomer peak d-spacing as a function of relative humidity, (b) shows the the d-spacing of the matrix knee versus RH, (c) shows the d-spacing of the matrix knee versus the ionomer peak, and (d) shows the ionomer peak FWHM versus d-spacing. Blue is data for N112, cyan for N115, and red for N211.

max (FWHM) in Fig. 22d, there does not appear to be a significant trend in any case. The same can be said for the matrix knee d-spacing versus RH in Fig. 22b. Obviously, a naive linear fit could be performed on the N211 dataset in Figs. 22a, 22c, and 22d as there are only two data points, but the first generation Nafion (both N112 and N115) are included together and could be fit to a linear function in both Figs. 22a and 22d; however, the error bars are large and the resulting fit would not be significant.

However, Kusoglu *et al.* [14] found a linear trend between ionomer peak d-spacing and

water uptake λ which describes the "nanostructural rearrangement in the membrane to accommodate more water molecules", similar to the plot of ionomer peak d-spacing against RH, although the RH to λ conversion is not completely linear. Even with access to both generations of Nafion, they did not compare the trend in each, rather reported only the data for N117.

Figure 22b is interesting because the matrix knee d-spacing does not change with RH for N112 or N211 and are at a similar value between 10 and 11 nm. However, N115 does vary from 12 to almost 14 nm, indicating there is a difference between the N115 and N112/N211 samples. N115 was also different from the other two when previously measured in vacuum, which may be due to the relative age of the samples because Nafion from before 2004 does not have fluorinated end groups [2].

Kusoglu *et al.* also found a linear trend between the matrix knee and ionomer peak d-spacing indicating that the "crystallites in the matrix are also moving apart slightly to accommodate the growth of the water domains" [3], and demonstrating that the first generation Nafion has a steeper amplitude than the second generation, indicating potentially different larger lengthscale reorganization due to the difference in manufacturing [3]. However, I observed only a significant difference with N115 as compared to the other samples which showed essentially a flat trend as in Fig. 22c.

Finally, Kusoglu *et al.* showed that the FWHM of the ionomer peak decreases with increasing ionomer peak d-spacing, indicating a slightly less disordered nanostructure [3]. However, I observed the opposite trend as shown in Fig. 22d, although the error bars on most of the data points are much too large to observe a significant trend.

Overall, the discrepancy between my data and those collected by Kusoglu *et al.* could be due to the difference in preconditioning, as in other cases, thickness differences, and difference in relative age of the samples.

V. CONCLUSION

The DVS measurements revealed that, while both N112 and N115 have essentially the same water uptake isotherms, N211 is drastically different. The first generation Nafion shows a nonlinear relationship between water uptake and RH with hysteresis between the adsorption and desorption isotherms, yet the second generation Nafion has a nearly linear

isotherm with little-to-no hysteresis. This difference is because the first generation Nafion's swelling is anisotropic relative to the second generation films [2], and may also be related to the age and thus degree of crystallinity of the samples.

The Xenocs humidity chamber for SAXS measurements provides humidity and temperature control for characterizing PEM films. However, there are limitations in the humidity control given that at high RHs the value oscillates around the setpoint value. Moreover, the Kapton windows provide some background scattering that may limit features observed around 0.4 $Å^{-1}$ in WAXS and below 0.06 $Å^{-1}$ in MAXS if the blank measurement is not done carefully. I avoided using sample holder position 5 because of its markedly different intensity profile in MAXS.

Using the humidity chamber to characterize two generations of Nafion PEMs showed that the majority of the SAXS profiles are similar, including under elevated humidity conditions. With increasing humidity above 30 and 40% RH, both Nafion generations showed an increase in the intensity of the ionomer peak centred near 0.2 $Å^{-1}$, due to water uptake on the ionic side chains. Only the second generation Nafion showed a slight change in peak centre from 0.18 to 0.15 $Å^{-1}$, perhaps because of the increased water uptake as observed in the DVS measurements. The ionomer peak change was the only change observed in the WAXS and MAXS Q ranges of the samples, and the change was reversible upon decreasing RH.

Both the first and second generation Nafion, specifically N112 and N211, showed little-to-no difference between a folded and a stacked, not folded sample in WAXS and MAXS, except for two layer films in the lower Q portion of MAXS at RH90%. Thus to eliminate any extra error introduced by folding, the samples should not be folded if the RH is to go above 60%.

Overall, the humidity chamber works well for Nafion measurements and should be applicable for other PEMs, ensuring that various factors such as sample thickness and transmission factor are considered. The next steps for this project are to perform more MAXS and WAXS measurements with the second generation Nafion as the RH equilibrates to verify whether the sample truly equilibrates after half an hour. Moreover, brand new samples of Nafion are on order and will be used to re-do many of the measurements written about here in order to eliminate the variable of relative age and crystallinity of the samples. Further, some measurements of the samples in the SAXS and possibly ESAXS and OWAXS should be performed to verify that the ionomer peak is the only feature that changes with humid-

ity. As well, other PEMs should be examined using the humidity chamber to evaluate the effectiveness of the chamber for those specific samples.

---

[1] Y. Wang, K. S.Chen, J. Mishler, S. C. Cho, and X. C.Adroher, "A Review of Polymer Electrolyte Membrane Fuel Cells: Technology, Applications, and Needs on Fundamental Research," Appl. Energy **88**, 981–1007 (2011).

[2] J. Peron, A. Mani, X. Zhao, D. Edwards, M. Adachia, T. Soboleva, Z. Shi, Z. Xie, T. Navessin, and S. Holdcroft, "Properties of Nafion NR-211 membranes for PEMFCs," J. Membr. Sci. **356**, 44–51 (2010).

[3] A. Kusoglu and A. Z. Weber,"New Insights into Perfluorinated Sulfonic-Acid Ionomers," Chem. Rev. **117**, 987–1104 (2017).

[4] L. Maldonado, J. C.Perrin, J. Dillet, and O. Lottin, "Characterization of Polymer Electrolyte Nafion Membranes: Influence of Temperature, Heat Treatment and Drying Protocol on Sorption and Transport Properties," J. Membrane Sci. **389**, 43–56 (2012).

[5] L. Rubatat, A. L. Rollet, G. Gebel, and O. Diat, "Evidence of Elongated Polymeric Aggregates in Nafion," Macromolecules **35**, 4050–4055 (2002).

[6] N. P. Blake, M. K. Petersen, G. A. Voth, and H. Metiu, "Structure of Hydrated Na-Nafion Polymer Membranes," J. Phys. Chem. B **109**, 24244–24253 (2005).

[7] H. Takata, N. Mizuno, M. Nishikawa, S. Fukada, and M. Yoshitake, "Adsorption Properties of Water Vapor on Sulfonated Perfluoropolymer Membranes," Int. J. Hydrog. Energy **32**, 371–379 (2007).

[8] P. W. Majsztrik, M. B. Satterfield, A. B. Bocarsly, and J. B. Benziger, "Water Sorption, Desorption and Transport in Nafion Membranes," J. Membrane Sci. **301**, 93–106 (2007).

[9] R. D. Andrade P. and C. E. Perez, "Models of Sorption Isotherms for Food: Uses and Limitations," Vitae **18**, 325–334 (2011).

[10] T. Mochizuki, K. Kakinuma, M. Uchida, S. Deki, M. Watanabe, and K. Miyatake, "Temperature- and Humidity-Controlled SAXS Analysis of Proton-Conductive Ionomer Membranes for Fuel Cells," ChemSusChem **7**, 729–733 (2014).

[11] W. H. De Jeu, *Basic X-Ray Scattering for Soft Matter* (Academic, Oxford University Press, 2016).

[12] E. Hecht, *Optics* (Academic, Addison Wesley, 2002).

[13] Xenocs *Operation Manual: Xenocs In-Situ Humidity Generator*, 2019.

[14] A. Kusoglu, S. Savagatrup, K. T. Clark, and A. Z. Weber,"Role of Mechanical Factors in Controlling the Structure-Function Relationship of PFSA Ionomers," Macromolecules **45**, 7467–7476 (2012).

[15] E. M. Schibli, A. G. Wright, S. Holdcroft, and B. J. Frisken, "Morphology of Anion-Conducting Ionenes Investigated by Xray Scattering and Simulation," J. Phys. Chem. B **122**, 1730–1737 (2018).

Description	1st N115 RH40%	2nd N115 RH40%	N115 RH80%
a_l [Å^{-p}cm^{-1}]	$(1.7 \pm 0.1) \times 10^{-3}$	$(2.9 \pm 0.1) \times 10^{-3}$	$(0 \pm 2) \times 10^{-3}$
p	-1.57 ± 0.02	-1.42 ± 0.02	-2.5 ± 0.5
r [cm^{-1}]	$(3.03 \pm 0.06) \times 10^{-2}$	$(3.08 \pm 0.03) \times 10^{-2}$	$(3.5 \pm 0.1) \times 10^{-2}$
a_1 [cm^{-1}]	0.262 ± 0.005	0.233 ± 0.005	0.70 ± 0.06
a_2 [cm^{-1}]	0.240 ± 0.007	$(4 \pm 1) \times 10^{-2}$	$(4.2 \pm 0.7) \times 10^{-2}$
a_3 [cm^{-1}]	$(7.6 \pm 0.7) \times 10^{-2}$	0.24 ± 0.01	0.23 ± 0.02
a_4 [cm^{-1}]	$(4.1 \pm 0.3) \times 10^{-2}$	$(8 \pm 1) \times 10^{-2}$	$(8.3 \pm 0.6) \times 10^{-2}$
a_5 [cm^{-1}]	$(1.07 \pm 0.07) \times 10^{-2}$	$(7.6 \pm 0.4) \times 10^{-3}$	0.26 ± 0.01
a_6 [cm^{-1}]	-	-	$(1.9 \pm 0.3) \times 10^{-2}$
b_1 [Å^{-1}]	$(5.22 \pm 0.08) \times 10^{-2}$	$(5.3 \pm 0.1) \times 10^{-2}$	$(4.6 \pm 0.1) \times 10^{-2}$
b_2 [Å^{-1}]	1.093 ± 0.003	1.19 ± 0.08	1.1883 ± 0.0008
b_3 [Å^{-1}]	0.91 ± 0.02	1.095 ± 0.005	1.094 ± 0.003
b_4 [Å^{-1}]	1.1868 ± 0.0007	0.93 ± 0.08	0.93 ± 0.02
b_5 [Å^{-1}]	0.350 ± 0.002	0.363 ± 0.002	0.1709 ± 0.0004
b_6 [Å^{-1}]	-	-	0.340 ± 0.006
c_1 [Å^{-1}]	$(5.8 \pm 0.1) \times 10^{-2}$	$(5.7 \pm 0.2) \times 10^{-2}$	$(6.9 \pm 0.3) \times 10^{-2}$
c_2 [Å^{-1}]	0.272 ± 0.004	0.1 ± 0.1	$(9.9 \pm 0.7) \times 10^{-2}$
c_3 [Å^{-1}]	0.542 ± 0.005	0.268 ± 0.007	0.270 ± 0.009
c_4 [Å^{-1}]	0.102 ± 0.003	0.5 ± 0.1	0.483 ± 0.005
c_5 [Å^{-1}]	0.132 ± 0.004	$(9.2 \pm 0.6) \times 10^{-2}$	$(9.3 \pm 0.4) \times 10^{-2}$
c_6 [Å^{-1}]	-	-	0.11 ± 0.01
s_1	0.17 ± 0.03	0.40 ± 0.05	0.30 ± 0.04
s_2	0.57 ± 0.04	1.0 ± 0.3	1.0 ± 0.1
s_3	0.11 ± 0.07	0.59 ± 0.03	0.59 ± 0.02
s_4	1.00 ± 0.06	0.1 ± 0.3	0.2 ± 0.2
s_5	0.5 ± 0.2	1.0 ± 0.2	0.06 ± 0.06
s_6	-	-	1.0 ± 0.3
χ^2_{red}	1.6	1.6	1.2

TABLE III: MAXS and WAXS N115 data fit parameters for Eq. 7.

Description	1st N112 RH30%	2nd N112 RH30%	N112 RH60%	N112 RH90%
a_l [Å^{-p}cm^{-1}]	$(5 \pm 6) \times 10^{-3}$	$(1.5 \pm 0.7) \times 10^{-2}$	0.21 ± 0.04	$(6 \pm 9) \times 10^{-2}$
p	-1.9 ± 0.3	-1.6 ± 0.1	-0.95 ± 0.07	-1.3 ± 0.2
r [cm^{-1}]	0.70 ± 0.02	0.67 ± 0.02	0.68 ± 0.06	0.80 ± 0.06
a_1 [cm^{-1}]	9.8 ± 0.3	9.0 ± 0.2	10.4 ± 0.1	17.8 ± 0.2
a_2 [cm^{-1}]	1.3 ± 0.2	4.9 ± 0.3	4 ± 1	1.6 ± 0.2
a_3 [cm^{-1}]	4.9 ± 0.3	1.3 ± 0.2	2 ± 1	4 ± 1
a_4 [cm^{-1}]	1.53 ± 0.03	1.52 ± 0.07	1.7 ± 0.3	2 ± 1
a_5 [cm^{-1}]	0.40 ± 0.02	0.35 ± 0.03	0.76 ± 0.09	6.4 ± 0.3
a_6 [cm^{-1}]	-	-	$(7 \pm 2) \times 10^{-2}$	0.2 ± 0.2
b_1 [Å^{-1}]	$(5.83 \pm 0.06) \times 10^{-2}$	$(5.97 \pm 0.06) \times 10^{-2}$	$(6.2 \pm 0.1) \times 10^{-2}$	$(6.29 \pm 0.08) \times 10^{-2}$
b_2 [Å^{-1}]	0.92 ± 0.02	1.087 ± 0.002	1.09 ± 0.05	1.1875 ± 0.0004
b_3 [Å^{-1}]	1.086 ± 0.001	0.92 ± 0.03	1.19 ± 0.05	1.09 ± 0.07
b_4 [Å^{-1}]	1.1863 ± 0.0003	1.1867 ± 0.0003	1.0 ± 0.1	0.96 ± 0.07
b_5 [Å^{-1}]	0.335 ± 0.003	0.352 ± 0.003	0.186 ± 0.003	0.172 ± 0.002
b_6 [Å^{-1}]	-	-	0.330 ± 0.006	0.30 ± 0.02
c_1 [Å^{-1}]	$(8.4 \pm 0.1) \times 10^{-2}$	$(8.1 \pm 0.1) \times 10^{-2}$	$(7.9 \pm 0.2) \times 10^{-2}$	$(8.5 \pm 0.1) \times 10^{-2}$
c_2 [Å^{-1}]	0.550 ± 0.008	0.281 ± 0.008	0.3 ± 0.1	0.107 ± 0.007
c_3 [Å^{-1}]	0.282 ± 0.009	0.55 ± 0.02	0.11 ± 0.08	0.3 ± 0.1
c_4 [Å^{-1}]	0.110 ± 0.003	0.108 ± 0.002	0.5 ± 0.2	0.5 ± 0.1
c_5 [Å^{-1}]	0.28 ± 0.01	0.26 ± 0.02	$(8.7 \pm 0.6) \times 10^{-2}$	$(9.1 \pm 0.2) \times 10^{-2}$
c_6 [Å^{-1}]	-	-	$(7 \pm 5) \times 10^{-2}$	0.10 ± 0.02
s_1	0.33 ± 0.04	0.32 ± 0.02	0.3 ± 0.1	0.2 ± 0.2
s_2	0.9 ± 0.1	0.42 ± 0.07	0.5 ± 0.2	1.0 ± 0.2
s_3	0.41 ± 0.09	0.8 ± 0.1	1.0 ± 0.3	0.5 ± 0.2
s_4	1.0 ± 0.2	1.00 ± 0.06	1.0 ± 0.2	0.8 ± 0.1
s_5	0.0 ± 0.1	0.0 ± 0.3	1.00 ± 0.06	0.6 ± 0.1
s_6	-	-	0.0 ± 0.5	1.0 ± 0.2
χ^2_{red}	1.8	2.0	1.9	2.3

TABLE IV: MAXS and WAXS N112 data fit parameters for Eq. 7.

Description	1st N211 RH30%	2nd N211 RH30%	N211 RH60%	N211 RH90%
a_l [Å^{-p}cm^{-1}]	$(5.3 \pm 0.9) \times 10^{-2}$	$(2.2 \pm 0.4) \times 10^{-2}$	0.163 ± 0.008	$(4 \pm 1) \times 10^{-2}$
p	-1.44 ± 0.04	-1.70 ± 0.05	-1.17 ± 0.01	-1.5 ± 0.1
r [cm^{-1}]	0.66 ± 0.02	0.67 ± 0.02	0.71 ± 0.02	0.77 ± 0.01
a_1 [cm^{-1}]	10.6 ± 0.2	10.4 ± 0.1	13.19 ± 0.09	23.3 ± 0.3
a_2 [cm^{-1}]	1.5 ± 0.1	5.0 ± 0.2	1.8 ± 0.2	1.44 ± 0.07
a_3 [cm^{-1}]	5.0 ± 0.2	1.4 ± 0.2	1.49 ± 0.05	4.2 ± 0.3
a_4 [cm^{-1}]	1.47 ± 0.04	1.51 ± 0.04	4.4 ± 0.2	1.8 ± 0.3
a_5 [cm^{-1}]	0.35 ± 0.02	0.39 ± 0.02	1.50 ± 0.03	8.51 ± 0.07
a_6 [cm^{-1}]	-	-	0.13 ± 0.01	0.25 ± 0.02
b_1 [Å^{-1}]	$(6.05 \pm 0.03) \times 10^{-2}$	$(6.05 \pm 0.03) \times 10^{-2}$	$(6.17 \pm 0.02) \times 10^{-2}$	$(5.99 \pm 0.01) \times 10^{-2}$
b_2 [Å^{-1}]	0.93 ± 0.02	1.086 ± 0.002	0.974 ± 0.009	1.1883 ± 0.0005
b_3 [Å^{-1}]	1.087 ± 0.001	0.93 ± 0.03	1.1876 ± 0.0005	1.087 ± 0.003
b_4 [Å^{-1}]	1.1884 ± 0.0005	1.1881 ± 0.0003	1.085 ± 0.002	0.96 ± 0.02
b_5 [Å^{-1}]	0.326 ± 0.003	0.326 ± 0.004	0.1830 ± 0.0004	0.1695 ± 0.0002
b_6 [Å^{-1}]	-	-	0.335 ± 0.001	0.315 ± 0.002
c_1 [Å^{-1}]	$(6.08 \pm 0.08) \times 10^{-2}$	$(6.22 \pm 0.07) \times 10^{-2}$	$(5.93 \pm 0.05) \times 10^{-2}$	$(6.50 \pm 0.05) \times 10^{-2}$
c_2 [Å^{-1}]	0.544 ± 0.007	0.274 ± 0.006	0.510 ± 0.003	0.102 ± 0.002
c_3 [Å^{-1}]	0.273 ± 0.005	0.55 ± 0.02	0.101 ± 0.001	0.270 ± 0.009
c_4 [Å^{-1}]	0.101 ± 0.001	0.104 ± 0.001	0.265 ± 0.006	0.49 ± 0.01
c_5 [Å^{-1}]	0.23 ± 0.01	0.30 ± 0.02	$(8.3 \pm 0.2) \times 10^{-2}$	$(8.43 \pm 0.06) \times 10^{-2}$
c_6 [Å^{-1}]	-	-	$(5 \pm 1) \times 10^{-2}$	$(8.8 \pm 0.6) \times 10^{-2}$
s_1	0.35 ± 0.03	0.27 ± 0.02	0.27 ± 0.02	0.13 ± 0.02
s_2	0.69 ± 0.07	0.42 ± 0.06	0.89 ± 0.09	1.00 ± 0.07
s_3	0.44 ± 0.06	0.7 ± 0.1	1.00 ± 0.01	0.51 ± 0.09
s_4	1.00 ± 0.02	1.00 ± 0.02	0.51 ± 0.07	0.66 ± 0.07
s_5	0.0 ± 0.2	0.0 ± 0.1	0.30 ± 0.09	0.39 ± 0.01
s_6	-	-	0.0 ± 0.4	1.0 ± 0.3
χ^2_{red}	2.1	2.3	2.0	2.5

TABLE V: MAXS and WAXS N211 data fit parameters for Eq. 7.